Materials Science and Engineering B 264 (2021) 114943

Contents lists available at ScienceDirect

Materials Science & Engineering B

journal homepage: www.elsevier.com/locate/mseb

Structure and physical properties of hydrogenated (Co + Al)-doped ZnO films: Comparative study with co-doped ZnO films

Yulia E. Samoshkina [a,*], Irina S. Edelman [a], Hsiung Chou [b,c], Hsien-Chi Lin [b], Gopeshwar D. Dwivedi [b], Dmitry A. Petrov [a], Sergey M. Zharkov [a,d], Galina M. Zeer [d], Maxim S. Molokeev [a,d]

[a] Kirensky Institute of Physics, Federal Research Center KSC SB RAS, 660036 Krasnoyarsk, Russia
[b] Department of Physics, National Sun Yat-sen University, Kaohsiung 80424, Taiwan, ROC
[c] Department of Applied Physics, National University of Kaohsiung, Kaohsiung 81148, Taiwan, ROC
[d] Siberian Federal University, 660041 Krasnoyarsk, Russia

ARTICLE INFO

Keywords:
(Co + Al)-doped ZnO
Co-doped ZnO
Diluted oxides
Thin films
Hydrogenation
Room temperature ferromagnetism

ABSTRACT

(Co + Al)-doped ZnO films have been synthesized by the RF magnetron sputtering. Films of this composition have first been obtained in mixed atmosphere of Ar + H_2. High hydrogen concentration of 20–50% has been used together with high enough substrate temperature of 450 °C. The used technological conditions affected the morphology, chemical composition, optical, electric, and magnetic properties of the films to an even more than in the case of Co-doped ZnO films synthesized under the same conditions and studied earlier. The films exhibit ferromagnetic behavior at room temperature with much greater magnetization and magneto-optical activity compared to the Co-doped films. At the same time, the hydrogenated films show an increase in electric conductivity in comparison with samples synthesized in the atmosphere of Ar + O_2. The magnetic nature of the hydrogenated films has been associated with the defect-related mechanism.

1. Introduction

Diluted magnetic oxides (DMO) based on ZnO are among the most promising candidates for spintronic applications, since they are wide-bandgap semiconductors, can exhibit ferromagnetism at room temperature and their magneto-electric properties can be controlled [1–4]. However, the origin of ferromagnetism (FM) in such materials is still under debate, as it critically depends not only on the nature of the doping elements but also on the conditions of the sample synthesis and the post-synthesis treatment. Many researchers use Co and Al as doping elements [5–10]. The first is for controlling the magnetic properties, and the second is for controlling the electrical conductivity. In the case of the ZnO films doped with Co and Al simultaneously, ferromagnetic behavior of the samples is also ambiguous because in some reports the magnetic moment of the sample increases with the Al introduction [5,7–9] in others it remains unchanged or even decreases [6,10].

As for the methods of preparation and post-synthesis treatment of the samples, hydrogenation of the doped ZnO has recently became increasingly popular. Theoretical [11,12] and experimental [13–16] studies have led to the conclusions that hydrogenation of the doped ZnO films uniquely induces/enhances FM behavior in the samples. Nevertheless, the ferromagnetism nature of the hydrogenated samples also remains controversial. In particular, ferromagnetism upon hydrogenation of the Co-doped ZnO films was explained in Refs. [6,17] by the formation of Co-H-Co complexes, authors of Refs. [18,19] associated it with the metallic Co clusters, mechanism of the FM state formation due to the defect-mediated environment was suggested in Refs. [20,21]. Such variety of theoretical interpretations may be partly due to the variety of the samples physical properties due to different hydrogenation methods. The main methods of hydrogenation are plasma treatment of the samples with the Ar-H_2 mixed gas [15,16], irradiation with a beam of hydrogen ions [21], the post-synthesis annealing in the H_2 atmosphere [19,22], and the radio frequency (RF) magnetron sputtering in the Ar-H_2 mixed gas environment [6,13]. Besides, the substrate temperature during the synthesis or post-synthesis treatment of the doped ZnO films play a key role in formation of their physical properties [22–24].

Recently, we have revealed exceptionally strong effect of the

* Corresponding author.
E-mail address: uliag@iph.krasn.ru (Y.E. Samoshkina).

https://doi.org/10.1016/j.mseb.2020.114943
Received 11 July 2020; Received in revised form 17 October 2020; Accepted 12 November 2020
Available online 25 November 2020
0921-5107/© 2020 Elsevier B.V. All rights reserved.

hydrogen introduction to the sputtering chamber on the structure and physical properties of the Co-doped ZnO films [25]. The films thickness decreased several times when Ar was partly replaced by hydrogen in concentrations from 20 to 50% compared to films sputtered from the same target in the Ar + O_2 atmosphere. Strong decrease in the Zn/Co ratio in the films, changes in the samples structure, electrical and magnetic behavior were observed simultaneously. The phenomenon was associated with the formation of gaseous ZnH_2 due to the reaction of hydrogen with Zn in the growing films under the conditions of the high substrate temperature (450 °C). Since this effect was observed for the first time, it was interesting to simulate a similar experiment for samples with other doping elements, in particular with a set of elements affecting both the magnetic and electrical properties of the films, for example Co + Al.

We know of only one report, in which the magnetic properties of the (Co + Al)-doped ZnO films hydrogenated using hydrogen plasma treatment were investigated [16]. Herewith, the treatment took place in atmosphere of the $Ar/H_2 = 9/1$ mixed gas, that is, at the essential lower hydrogen concentration comparing to Ar/H_2 ratio from 4/1 to 1/1 used in [25]. The Al doping in Ref. [16] suppressed the hydrogen-mediated ferromagnetism in Co-doped ZnO films.

In connection with the above, we synthesized the (Co + Al)-doped ZnO thin films by the RF magnetron sputtering in mixed atmospheres of Ar + 20–50% H_2 and Ar + 20% O_2 exactly at the same conditions used for synthesis of the Co-doped ZnO films in Ref. [25]. The morphology, chemical composition, crystal structure, optical transmission, electrical resistivity, and magnetic properties of the samples were investigated. The data were analyzed comparing them with that obtained earlier for the Co-doped ZnO films [25]. The role of hydrogen in the formation of magnetic and electrical properties of the samples was considered basing on this analysis.

2. Material and methods

2.1. Samples synthesis

The (Co + Al)-doped ZnO (CAZO) films were grown on a glass substrate by the standard RF magnetron sputtering system using the two-inches $Zn_{0.93}Co_{0.05}Al_{0.02}O$ target. The target was synthesized from high purity ZnO (99.999%), Al_2O_3 (99.997%), and Co_3O_4 (99.9985%) by a standard two steps solid state reaction method. All of three raw materials were weighted according the mole ratios. ZnO and Al_2O_3 weighted powders were mixed and calcined at 1300 °C for 10 h under the flow of oxygen. The calcined powder was ground and ready for another calcine process. After of two times of high temperature calcined, the powder was proportionally mixed with Co_3O_4. 5% of polyvinyl alcohol (PVA) binder mixed with the final powder which was then pressed into two inches pallet. The pallet was heating up slowly with a ramp rate of 1 °C/min to 600 °C and remained for 6 h to decompose and evaporate PVA out from the target. The pallet was continuously and slowly heating up to 860 °C and stayed at this temperature for 10 h to form target. The final target was cooled down slowly to room temperature. The films deposition was carried out at a total pressure of 30 mTorr and a forward RF power of 80 W at the substrate temperature 450 °C for 20 min. Five samples were deposited with the following mixed gas in the chamber: Ar + 20% O_2, Ar+ (20%, 30%, 40%, 50%) H_2, samples CAZO1-CAZO5, respectively. For the comparison, the Co-doped ZnO (CZO) films were deposited from the $Zn_{0.95}Co_{0.05}O$ target exactly at the same conditions – samples CZO1-CZO5, respectively.

2.2. Methods

The films cross-section was obtained using the high-resolution transmission electron microscope (TEM). A two-beam focusing ion beam with a final trim energy of 5 keV was used. Analysis of the films structure was studied using field emission gun high-resolution TEM (Tecnai F20 G2 MAT S-TWIN).

The compositional analysis was performed by a field emission electron probe microanalyses (EPMA) using the JEOL JXA-8530F. An electron beam was incident on the surface of the films on a large area of 100 × 100 μm^2 and few points of around 1 × 1 μm^2, and their X-ray wavelength dispersive spectra (WDS) were collected for compositional analysis. To enhance the confidence on the compositional probing, several spectra were collected for around six minutes for every detection area. Final quantity analysis on Zn and Co was done by averaging these spectra.

A JEOL JSM-7001F scanning electron microscope (SEM) was used to investigate the films surface. The films thickness and elemental composition were examined also by X-ray fluorescent analysis (XRFA) using a spectrometer S4 PIONEER (Bruker).

X-ray diffraction (XRD) data were collected at room temperature with a Bruker D8 ADVANCE powder diffractometer (Cu-Kα radiation) and linear VANTEC detector. To increase the intensity of the powder pattern, a detector slot with a diameter of 2 mm was used. The step size of 2θ was 0.016°, and the counting time was 7 sec per step. Rietveld refinement was performed by using TOPAS 4.2.

The electrical resistivity of the films was investigated at room temperature using the standard four-point probe technique. The optical transmittance was measured at room temperature with N&K spectrometer.

The magnetic properties of the samples were studied by magnetic circular dichroism (MCD) at the optical frequencies. The MCD effect reflects the magnetic behavior of the sample, since this effect is linear function of the sample magnetization in the magnetic field. MCD was measured in the normal geometry: an external magnetic field vector and the light beam were directed normal to the films plane. Thus, during the measurement process, the change in the projection of the magnetic moment of the sample on the direction normal to its plane was recorded The modulation of the polarization state of the light wave from the right-hand to the left-hand circular polarization relatively to the magnetic field direction was used. The MCD value was measured by the formula $\Delta k = (D_+ – D_-)/d$, where D_+ and D_- are the optical density of the films for right and left polarized waves, and d is the films thickness. Measurements were carried out in the spectral range 1.2–4.5 eV in a magnetic field up to 13 kOe at the temperature 300 K. The measurement accuracy was about 10^{-4}, and the spectral resolution was 20–50 cm^{-1} depending on the wavelength.

3. Results and discussion

3.1. Morphology, crystal structure, and chemical composition

The thickness of the CAZO films determined by XRFA is presented in Table 1 in comparison with the thicknesses of the CZO films. The thickness of CAZO1 and CZO1 was 130 and 160 nm, that is, the deposition rate for these films was about 0.11 и 0.13 nm/sec, respectively. These values are within the deposition rates ~0.04 nm/sec and ~0.8 nm/sec obtained by different authors for the Co-doped and Al-doped ZnO films synthesized by the RF sputtering in the pure Ar atmosphere under slightly different technological conditions [19,26,27]. Authors of these reports noted a decrease in the films deposition rate approximately by about 15–30% when hydrogen was added into the sputtering chamber. The value of the films deposition rate depended on the deposition power and the hydrogen flow rate.

In our case, the sharp decrease in the films thickness (more than twice) at the transition from the Ar + O_2 to the Ar + H_2 atmosphere and its slower diminution with the further increase in the hydrogen concentration in the gas mixture is characteristic for both sets of the films. The reduction of the films thickness with the increasing hydrogen concentration is confirmed by TEM images obtained for several samples. Examples of the cross-section TEM image for the CAZO1 and CAZO5 samples are shown in Fig. 1. The results of both types of measurements

Table 1
The films thickness according to XRFA, Zn/Co ratio according to XRFA, as well as EPMA data, and electrical resistivity for CAZO and CZO films.

Sample	Gas mixture	Doping elements	Film thickness, nm	Zn/Co		Resistivity, Ohm*cm
				(XRFA)	(EPMA)	
CAZO1	Ar + 20% O_2	Co + Al	130	18.5	22	Over $14.8*10^2$
CZO1		Co	160	19.2	26.72	Over $22.7*10^2$
CAZO2	Ar + 20% H_2	Co + Al	36.9	4.1	4.58	$4.5*10^{-2}$
CZO2		Co	71.7	4.3	4.23	$11.8*10^{-2}$
CAZO3	Ar + 30% H_2	Co + Al	18.8	2.6	2.19	$4.6*10^{-1}$
CZO3		Co	53.5	3.6	3.05	$6.4*10^{-2}$
CAZO4	Ar + 40% H_2	Co + Al	18	2.5	~0.75	$4.1*10^{-1}$
CZO4		Co	37	2.9	2.09	$1.6*10^{-2}$
CAZO5*	Ar + 50% H_2	Co + Al	14.1	–	~0.70	$6.4*10^{-1}$
CZO5		Co	31.6	2.6	1.49	$1.5*10^{-2}$

*) Zn/Co ratio was not determined for the film because of its very small thickness.

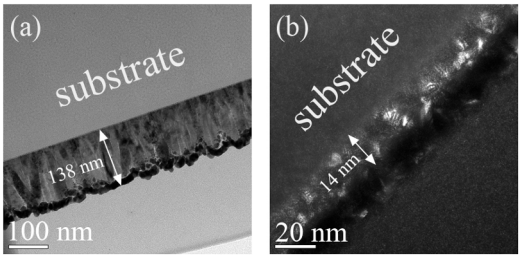

Fig. 1. TEM images of the cross-sections of CAZO1 (a) and CAZO5 (b) films.

match very well (Fig. 2). Note that despite the same synthesis conditions, for all samples of the CAZO series, the films thickness is less than that of the CZO series. Probable, the Al admixture diminishes the sputtering rate of the target.

The decrease in the films thickness with the increase in the hydrogen concentration is accompanied by a decrease in Zn/Co ratio in the films (Table 1). For all CAZO and CZO samples, the Zn/Co ratio was determined by the XRFA and EPMA data. The obtained data correlate well with each other. According to the data, the Zn and Co content in the CAZO1 and CZO1 samples is close to that in the sputtered targets (18.6 for CAZO and 19 for CZO). This ratio decreases with the transition from the gas mixture Ar + O_2 to Ar + H_2 and with the subsequent increase in the H_2 concentration in the sputtering chamber following approximately the same regularity as the decrease in the films thickness (insert in Fig. 2). It means that the films thickness decreases due to a decrease in the Zn amount in them.

It should be noted that the relative Al content in the CAZO2-CAZO5 samples also increases with increasing H_2. Percentages of Co and Al in the CAZO and CZO films calculated under the assumption that the ratio Co/Al remains constant are collected in Table 2.

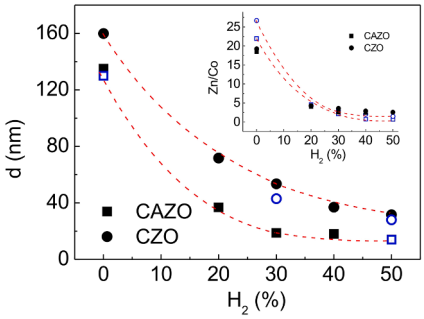

Fig. 2. Dependence of the CAZO and CZO films thickness on the hydrogen concentration in the sputtering chamber (filled symbols – the data obtained by XRFA, open symbols - the data obtained by TEM). Insert: dependence of the Zn/Co ratio in the CAZO and CZO samples on the hydrogen concentration in the sputtering chamber (filled symbols – the data obtained by XRFA, open symbols – the data obtained by EPMA). The dash lines are for guide to eye.

The surface images obtained by SEM for the CAZO2-CAZO5 samples are shown in Fig. 3. The granular structure is characteristic of the CAZO2-CAZO4 films and typical for the ZnO samples in general [10,28]. Herewith, the granules size decreases with the hydrogen concentration increase. For the CAZO5 films, at a given scale the structure is not defined. All CZO films have granular structure, which persists for the CZO5 film also (Fig. 4).

XRD patterns for the CAZO1, as well as CZO2 and CZO3 films are presented in Fig. 5. For CZO1-CZO5 films, the grazing incidence angle X-ray diffraction (GIXRD) patterns were presented in our previous paper [25], where the intense diffraction peaks were observed corresponding to the (100), (002), and (101) crystal planes of ZnO indicating the polycrystalline structure of the films. All observed diffraction peaks for CAZO1 film also correspond to the ZnO lattice with a hexagonal wurtzite crystal structure $P6_3mc$. Therefore, the ZnO crystal structure [29] was taken as a starting model for the Rietveld refinement. Refinements were stable and gave low R-factors (Table 3). (R-factor is a figure of merit quantifying the quality of the fit between calculated and experimental patterns, which is used to characterize the quality of refinement). For the CAZO1 sample, only c-cell parameter was refined (Table 3), indicating the pronounced texture in the film what explains extremely high intensity of the reflections (Fig. 5a). For the CZO2 and CZO3 samples, the most intense diffraction peaks correspond to (100), (002), and (101) planes of ZnO, indicating the polycrystalline structure of the films in accordance with the data in Ref. [25]. The intensity of these peaks decreases strongly with increasing hydrogen concentration. Such a behavior indicates a decrease in the crystallites size in the samples and the degree of their preferential orientation with an increase in the hydrogen concentration as confirmed by the data presented in Table 3. Since the average crystallites size for the CZO2 and CZO3 films is within 10 nm, we can suggest that the crystallites size is even smaller and preferred orientation coefficient is higher in CZO4 and CZO5 samples, as

Table 2
Percentage of Co and Al in the CAZO and CZO films calculated using the XRFA data and a system of equations: Co + Zn = 100%, Co + Al + Zn = 100%, Co/Al = 2.5.

Sample	Gas mixture	Doping elements	Zn/Co (XRFA)	Co (%)	Al (%)
CAZO2	Ar + 20% H_2	Co + Al	4.1	18.3	7.3
CZO2		Co	4.3	19	
CAZO3	Ar + 30% H_2	Co + Al	2.6	25.3	10.1
CZO3		Co	3.6	21.8	
CAZO4	Ar + 40% H_2	Co + Al	2.5	25.5	10.2
CZO4		Co	2.9	25.7	
CAZO5*	Ar + 50% H_2	Co + Al	–	–	–
CZO5		Co	2.6	28.1	

*) Zn/Co ratio was not determined for the film because of its very small thickness.

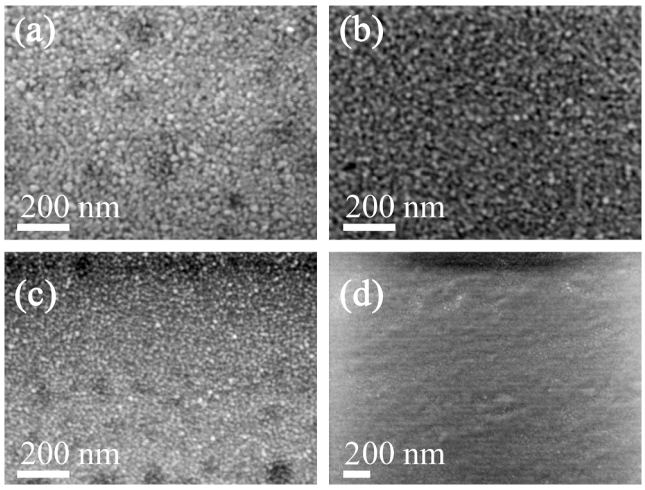

Fig. 3. SEM images of the CAZO2-CAZO5 (a-d) films surface.

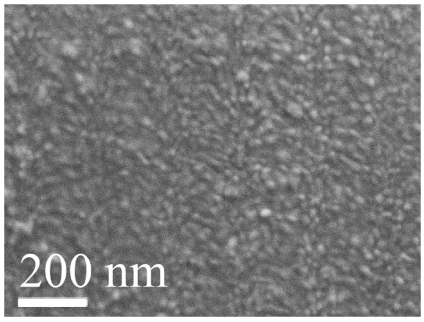

Fig. 4. SEM image of the CZO5 film surface.

well as CAZO2-CAZO5, for which reflexes are practically not observed.

Thus, the introduction of hydrogen into the sputtering chamber not only leads to a decrease in the films thickness and a change in their chemical composition compared with the composition of the target, but also strongly affects crystal structure of the samples. Taking into account the increase in the relative Co content in the hydrogenated CAZO and CZO samples (as well as the relative Al content in the CAZO2-CAZO5 films) with the increasing hydrogen concentration (Table 2), one could expect the formation of secondary phases related to Co and Al. However, no other crystal phases associated with Co and Al are observed in the XRD patterns. Such secondary phases were also not observed by more sensitive GIXRD method for all CZO films [25].

A decrease in the thickness and change in chemical composition of the doped ZnO films fabricated under certain technological conditions were traced earlier by several authors. Conditions closest to those used in the present research were presented in Refs. [22, 23, and 30]. The Co-doped ZnO films were prepared with the pulsed laser deposition technique in an oxygen-deficient ambient at the substrate temperatures from 300 to 600 °C [23]. It was found that the Co content in the films was higher than in the target (15% instead of 10%) at substrate temperatures of 400 °C and above. It was explained by the re-vaporization of the Zn atoms in greater number than Co atoms. The Mg^{2+} and Ga^{3+} co-doped ZnO films deposited with magnetron sputtering at various hydrogen flow rates and substrate temperature of 250 °C were studied in Ref. [30]. The films thickness decreased almost twice with increasing the H_2 flow rate (max $H_2/(Ar + H_2)$ ratio was 18%). The authors explained this by the fact that the deposition rate decreases with increasing the introduction of hydrogen in the chamber for the reason that H_2 is lighter than Ar. Besides, they found that the Zn atomic percent in the films decreased (by about 6% at the maximal H_2 content) and the Mg atomic percent

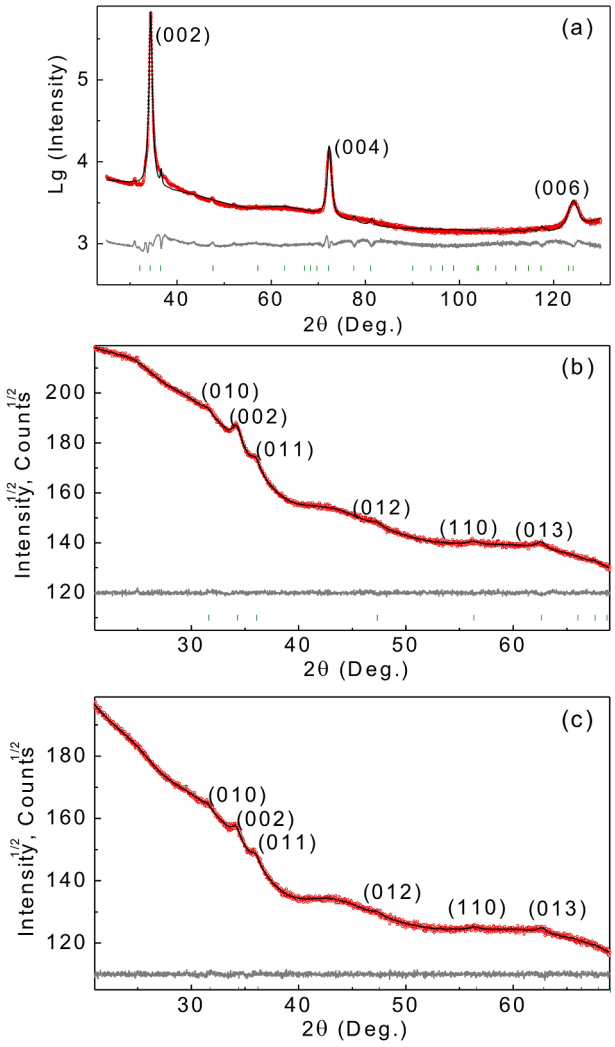

Fig. 5. Difference Rietveld plot of XRD patterns for the CAZO1 (a), CZO2 (b), and CZO3 (c) films. For the CAZO1 sample (a), logarithm of intensity is plotted along the ordinate due to the extremely high intensity of reflexes from the film. For the other two samples deposited in a hydrogen atmosphere (b and c), the square root of the intensity is plotted along the ordinate axis in order to distinguish very weak reflexes.

Table 3
Structural parameters of the samples and main parameters of the refinement. R_{wp} is the weighted profile residual and R_p is profile residual (reliability factor).

Sample	CAZO1	CZO2	CZO3
Space group	$P6_3mc$	$P6_3mc$	$P6_3mc$
a, Å	3.22*	3.264 (4)	3.251 (3)
c, Å	5.2324 (7)	5.223 (8)	5.207 (7)
V, Å^3	46.983 (6)*	48.2 (1)	47.7 (1)
Average crystallites size, Å	–	101 (3)	94 (6)
2θ-interval, Degrees	25–130	20–70	20–70
Preferred orientation coefficient **	0.1	0.671 (4)	0.727 (7)
R_{wp}, %	6.44	0.63	0.71
R_p, %	4.30	0.49	0.56

* Cell parameter *a* was fixed due to strong preferred orientation on (001) plane and almost absence of (*hk*0) reflections. Cell volume was calculated using not refined *a* cell parameter.
** Absence of preferred orientation gives coefficient equal to 1.

increased gradually (by about 30% at the maximal H_2 content) with increasing the H_2 flow rate. The Ga atomic percent remained almost unchanged. The Al-doped ZnO films prepared by magnetron sputtering

under pure Ar atmosphere and then annealed under H_2 atmosphere at temperature from 300 to 625 °C were studied in Ref. [22]. It was established that when annealing above 450 °C, the films thickness decreased by about 10%, and the relative Al content in the samples increased approximately 2 times. In this connection, a large number of generated zinc vacancies (V_{Zn}) was attributed to the hydrogen etching effect. Thus, the change in parameters of the films under the effect of hydrogen was previously mentioned, but not to such a great extent as in our case. Evidently, the combination of the high hydrogen concentration in the sputtering chamber in the process of the films deposition and large enough substrate temperature were the main factors responsible for the extremely low CAZO and CZO films thickness and the low Zn/Co ratio.

As it was mentioned above, the CZO films were synthesized by us earlier under the same technological conditions as in the present study [25]. Analyzing possible origin of the extremely strong hydrogen effect on the films thickness and chemical composition, we proposed a reaction of hydrogen with the growing Co-doped ZnO film in the process of its deposition. Formation of a gaseous zinc hydride as a result of the reaction (1) leads to a decrease in the Zn amount in the film. In additional, the reaction intensity increases with an increase in the hydrogen concentration in the sputtering chamber that leads to further reduction of the Zn amount in the films. Such assumption was based on the results of reports [31,32] and especially on the report [33], where the special experiment was carried out. A zinc rod was placed into an alumina tube and heated it to 470 °C. Pure hydrogen floated slowly through the tube, the DC discharge (3 kV, 333 mA) was applied between two electrodes located inside the water-cooled ends of the alumina tube. The ZnH_2 gas was detected directly in the tube with the help of infrared spectroscopy through the special windows in the tube. Our experimental conditions (the substrate temperature 450 °C and H_2 migrating between the target and substrate) are close to those used in [33]. Therefore, the reaction (1) is quite possible in the case of the CAZO films. This reaction explains the hydrogen effect on the morphological characteristics of the samples and redistribution of the relative content of Co, Al and Zn in the films. However, the noticeable stronger decrease in the CAZO films thickness comparing to that of the CZO films (see, Table 1) induces one to think of any additional mechanism enhancing the hydrogen effect in CAZO film formation. This mechanism is not clear now.

$$ZnO + 2H_2 \rightarrow ZnH_2 + H_2O, \quad (1)$$

3.2. Electrical and optical properties

The changes in the morphology and chemical composition of the films caused by the hydrogen addition into the sputtering chamber are accompanied by changes in their physical properties. As can be seen from Table1 and Fig. 6, the electrical resistivity is of about $14.8*10^2$ Ohm*cm for the CAZO film deposited in Ar + O_2 atmosphere and even higher for CZO1 sample. This magnitude exceeds the resistivity of the films deposited in an argon, oxygen or vacuum atmosphere by 4–6 orders [22,34,35]. For the CAZO2 and CZO2 films deposited in Ar + H_2 atmosphere, the resistivity value is lower by 4 orders of magnitude compared to the CAZO1 and CZO1 samples. Then, with increasing hydrogen concentration in the sputtering chamber, the resistivity of the CZO3-CZO5 films falls monotonously within the same order, and the resistivity of the CAZO3-CAZO5 films rises non-monotonically.

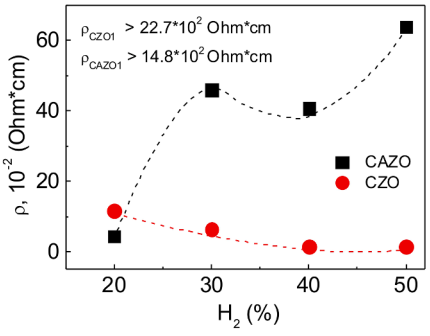

Fig. 6. Dependence of the resistivity value on the hydrogen concentration for the CAZO and CZO films. The dashed lines are the guides for eye.

The four-order increase in the conductivity of the CAZO and CZO films synthesized in a hydrogen-enriched atmosphere is apparently associated with shallow donors, the amount of which increases with increasing hydrogen concentration. Most of the authors conclude that ZnO films can contain the shallow donors, such as oxygen vacancies (V_O) and zinc interstitials (Zn_i) [22,23,34–36]. In addition, hydrogenated ZnO films can contain donor H^+ when it occupies interstitial positions (H_i) or vacant oxygen sites (H_O) [22,24,30,37]. In the case of the Al-doped ZnO samples discussed in literature, Al acts as the dominant donor because it generates free electrons [8,10,22,24,34,35,38]. By comparing the resistivity between the CAZO2 and CZO2 films (Table 1, Fig. 6), one can suppose that Al in the CAZO2 sample acts as the dominant donor. However, already for the CAZO3 sample, resistivity increases noticeably despite an increase in the hydrogen concentration during the sputtering process, which in principle should lead to a decrease in resistivity. For the hydrogenated CAZO and CZO samples, two competing mechanisms effect strongly on the resistivity, namely the appearance of the electron donors and the grain boundary scattering. As it is seen from the TEM images and the XRD patterns, crystal structure of the films deteriorates with increasing H_2 concentration, and the samples thickness decreases (see Section 3.1). Obviously, the films have the greater defects density in the grain boundaries at thinner thickness that increases the grain boundary scattering of free electrons, which lead to increase in the resistivity. In the case of the CAZO-CAZO5 films, grain boundary scattering probably dominates.

The optical transmittance spectra for all samples are presented in Fig. 7(a and c). The CAZO1 and CZO1 films demonstrate about 80–90% transparency in the region 450–1000 nm, while the transparency of the hydrogenated samples is lower despite their significantly smaller thickness. It is noteworthy that the transparency value is almost the same for the CAZO2-CAZO5 films and is 50% in the visible region, whereas the transparency value for the CZO2-CZO5 films decreases from 55 to 35% with the increase of the hydrogen concentration during films deposition.

The optical absorption (α) spectra and the band gap (E_g) for the studied films were calculated from the transmittance spectra in the strong absorption region, where reflection loss can be neglected. Data were obtained using the Beer-Lambert law $\alpha = (1/d)*\ln(1/T)$, where T is transmittance and d is film thickness, along with the Tauc model $(\alpha h\nu)^2 = A(h\nu - E_g)$, where $h\nu$ is the energy of the incident photon, and A is the energy-independent constant. The obtained E_g value for the CAZO1 film is 4.1 eV (insert in Fig. 7b). At the same time, for the CZO sample also deposited in Ar + O_2 atmosphere, E_g was found to be ~3.3 eV (insert in Fig. 7d) that is close to 3.31 eV for bulk ZnO [39] and 3.26 eV for ZnO micro-rods [40]. For the hydrogenated CAZO films, the E_g value is almost constant and is ~ 4.3 eV (Fig. 7b). In the case of the hydrogenated CZO samples, E_g increases from 4.3 to 4.5 eV with the growth of the hydrogen concentration in the sputtering chamber (Fig. 7d).

The E_g broadening was observed earlier both for the Al-doped ZnO samples and for the non-doped ZnO samples (without [34,38,41] or with [22,24,38,42] hydrogen participation). Such behavior was explained by the E_g dependence on the microstructure and conductivity of the material, including the grain size, strain, and carrier concentration. The small grain size leads to an increase in the contribution of the grain boundary scattering into the sample optical properties, which leads to a broadening of the optical band gap [43]. The compressive lattice strain increases the optical band gap, while the tensile lattice strain decreases it [41]. An increase in the carriers concentration in the samples can also effect on an increase in the E_g value due to the Burstein–Moss (BM) effect, which is caused by the filling the lowest states of the conduction

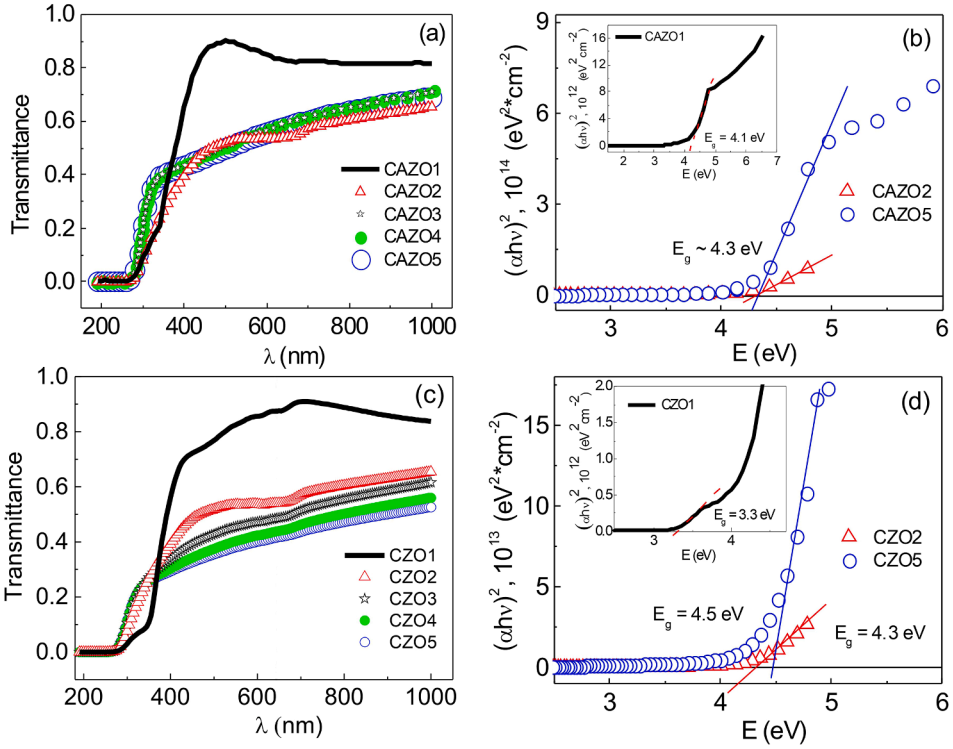

Fig. 7. Optical transmittance (T) spectra for the CAZO (a) and CZO (c) films. Plots of $(\alpha h\nu)^2$ vs photon energy (E) for the CAZO (b) and CZO (d) films synthesized in Ar + H_2 atmosphere. Inserts: plots of $(\alpha h\nu)^2$ vs photon energy (E) for the CAZO (b) and CZO (d) samples synthesized in Ar + O_2 atmosphere.

band with free electrons, creating shift of the Fermi level [44]. It should be noted that the E_g value in the reports of many authors does not exceed 3.8 eV. E_g slightly above 4 eV was observed in Ref. [34] for the Al-doped ZnO samples deposited in vacuum and in Ref. [45] for the (Cu, K) doped ZnO films fabricated by chemical bath deposition method. In our previous report [25], we found that the E_g value increases up to 4.6 eV for the hydrogen-doped ZnO films synthesized under the same conditions as CAZO and CZO. Considering the structural data of the hydrogenated ZO [25], CZO, and CAZO samples and the E_g value for the CAZO1 film equal to 4.1 eV, we are inclined to conclude that E_g for the studied films is mainly controlled by the carrier concentration and grain boundary scattering.

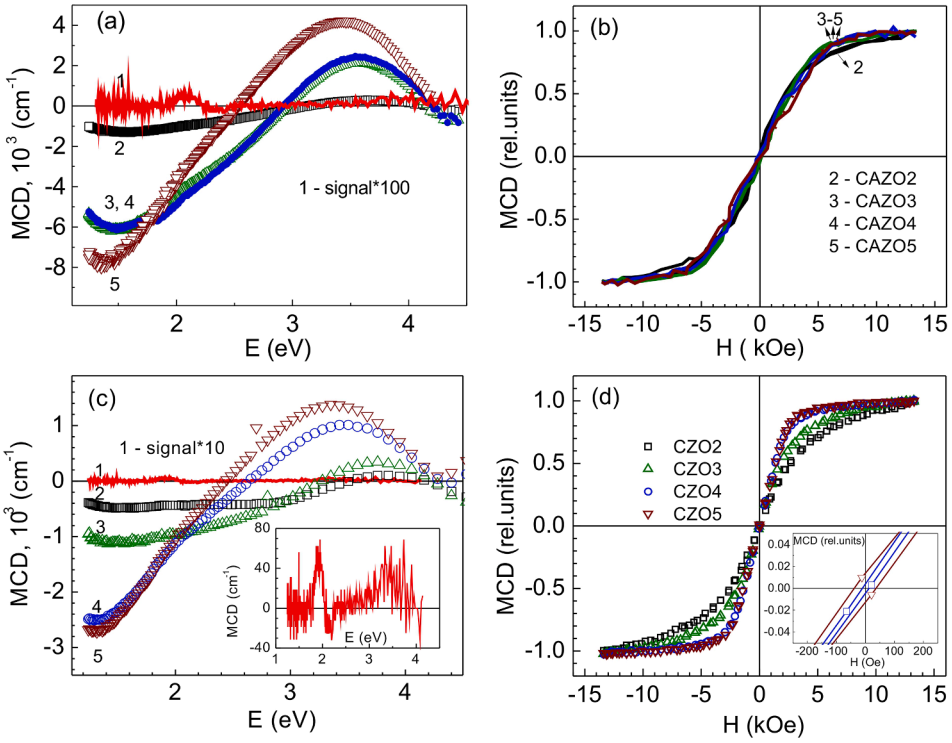

Fig. 8. a – MCD spectra for the CAZO1-CAZO5 samples, curves 1–5, respectively (H = 13 kOe, T = 300 K). b – MCD hysteresis loops for the CAZO2-CAZO5 samples (E = 1.55 eV, T = 300 K). c – MCD spectra for the CZO1-CZO5 samples, curves 1–5, respectively (H = 13 kOe, T = 300 K) [25]. d – MCD hysteresis loops for the CZO2-CZO5 samples (E = 1.55 eV, T = 300 K) [25]. Insert in c: the magnified MCD spectrum for the CZO1 film. Insert in d: low field parts of the MCD hysteresis loops for the CZO4 and CZO5 samples. The normalized MCD values are shown in parts b and d: the MCD value in the maximal magnetic field was taken as a unit for each sample.

3.3. Magnetic circular dichroism

MCD spectra for all CAZO and CZO films are shown in Fig. 8, parts a and c. The MCD spectrum shapes for CAZO1 and CZO1 samples are identical (Insert in Fig. 8c). Herewith, the MCD signal is very low and linear in the magnetic field (not shown). The hydrogen addition during the deposition of the studied films leads to strong changes in the MCD spectra (curves 2–5 in Fig. 8, parts a and c). For the hydrogenated CAZO and CZO samples, the spectra shape and their changes with the increase in the hydrogen concentration are also similar. This behavior indicates the same electronic structure for the hydrogenated CAZO and CZO samples. However, the MCD signal for the CAZO films is noticeably higher than that for the CZO samples. The largest difference between MCD signals in the spectral extremes is observed for CAZO3 and CZO3 – of about 6 times.

Earlier, MCD was applied by several authors to study magnetization of the diluted semiconductor films, e.g., for the hydrogenated Co-doped ZnO films [6,13]. The MCD dependences on an external magnetic field for the CAZO and CZO films are shown in Fig. 8, parts b and d, correspondingly. The presented dependences are typical for ferromagnetic films when they are magnetized in the direction perpendicular to the plane of the film. Recall that due to the peculiarities of the MCD measurement (the light beam propagates perpendicular to the film plane), it is used to record the magnetization curve in the direction perpendicular to the film plane, i.e., the z-direction. The magnitude of the M_z component for each value of the field H is determined by the competition between the energy of the magnetic moment interaction with the magnetic field and the energy of the demagnetizing field H_d, which for the described geometry is $H_d = -4\pi M_z$. A film become magnetized to saturation in magnetic field $H_s = 4\pi M_s$, where M_s is the saturation magnetization.

MCD (H) curves for the CZO4 and CZO5 films are very close to this ideal case. The coercivity for the CZO2-CZO5 samples (about 10–40 Oe, Insert in Fig. 8d) is negligible, and we can call the magnetization curves hysteresis-free, as noted in Ref. [46]. For other samples, the curves MCD (H) are smoother, which may be due to different granular morphologies of the films confirmed by the SEM data. Thus, the dependence of MCD on the magnetic field confirms definitely the room temperature ferromagnetic state for the studied films.

In our previous study [25], we considered formation of metallic Co clusters as one of possible mechanisms responsible for the long-range magnetic order in the CZO2-CZO5 samples. This assumption was supported by data of the X-ray absorption spectroscopy revealed the presence of metallic Co clusters in the samples. At the present paper, a growth of the MCD signal at extremes with increasing the relative Co content in the film is observed for both series (CAZO and CZO). This behavior indicates an increase in the samples magnetization with increasing the relative Co content in them and does not contradict this model. However, the higher magnetization of CAZO comparing CZO films with practically the same cobalt content in each pair of the samples deposited at the same hydrogen concentration (Table 2) makes us think of other mechanisms responsible for the ferromagnetic state of the films.

The films granular structure mentioned above may indicate a high density of defects in these samples. Thus, we consider the model of the bound magnetic polarons (BMP) in diluted n-type oxides suggested in Ref. [47]. This model proposes that in these materials the indirect ferromagnetic exchange between 3d electrons of the doped ions is mediated by shallow donor electrons that form bound magnetic polarons, which overlap to create a spin-split impurity band. Obviously, a certain specific density of defects is needed to induce long-range magnetic order. This density determines the Curie temperature. A further increase in the density of defects should lead to the involvement of a larger volume of the sample in an ordered state and thereby to an increase in magnetization, which is observed when passing from the CZO to CAZO films. The ferromagnetism of the Cu-doped, Mn-doped, and Co-doped ZnO samples was explained within the BMP model in Refs. [48–50].

At the same time, some authors attributed an enhanced magnetism induced by the Al introduction into the Co-doped ZnO films to carrier-mediated exchange mechanism [7,9,10]. It should be noted that ferromagnetism of the doped ZnO thin films was also explained by a combination of the BMP mechanism and carrier-mediated interaction of the magnetic moments [51,52].

Now it is difficult to incline to one or another specific mechanism that could explain unambiguous ferromagnetic behavior of the investigated films. Clarification of the relationship between doped atoms and intrinsic defects of the films requires further studies, as well as determination of the optimal conditions of the samples synthesis (hydrogen concentration and substrate temperature) with the best properties for real applications.

4. Conclusions

When synthesizing samples by RF-magnetron sputtering, the combination of the high hydrogen concentration in the sputtering chamber with the substrate temperature of 450 °C strongly affects the morphology, crystal structure, chemical composition, optical, electrical, and magnetic properties of the (Co + Al)-doped ZnO films. In contrast to the (Co + Al)-doped ZnO films synthesized in the atmosphere of Ar + O_2, the thickness of hydrogenated films is 3–9 times less depending on the hydrogen concentration, and the Zn/Co ratio decreases up to ~1. In additional, the relative Al content in the samples increases from 2% to ~10%. Such changes, which were also observed earlier in the case of Co-doped ZnO films, are explained by the chemical reaction of hydrogen with Zn in the growing films. As a result of the reaction, gaseous ZnH_2 is formed, which is removed from the chamber together with the pumped working gases.

The electric conductivity of the (Co + Al)-doped ZnO films synthesized in the Ar + H_2 atmosphere improves significantly comparing to the films deposited in the Ar + O_2 atmosphere. However, the electrical resistivity of the films remains still higher than in most cases doped ZnO samples. This behavior is explained by the dominance of grain boundary scattering in the films. It was also shown that the optical band gap for the studied samples has quite large values in the range of 4.1–4.3 eV. The E_g values are mainly associated with carrier concentration and grain boundary scattering. The optical transparency for the hydrogenated films is about 50% in visible region.

Similar to the magnetic behavior of the Co-doped ZnO films synthesized under the same conditions, the (Co + Al)-doped ZnO films exhibit ferromagnetic almost hysteresis-free behavior at room temperature. In additional, the magnetization value for the (Co + Al)-doped ZnO films is several times higher than for the Co-doped ZnO samples. We assume that the observed ferromagnetism of the films associated with the defect-related mechanism. The results obtained give insight about the structure and physical properties of diluted oxides, such as Co and (Co + Al)-doped ZnO films synthesized with RF magnetron sputtering at very high hydrogen concentration and the substrate temperature, as well as provide a guidance to create new materials for the spintronics and spin-electron devices.

Declaration of Competing Interest

The authors declare that they have no known competing financial interests or personal relationships that could have appeared to influence the work reported in this paper.

Acknowledgements

H.C. thanks the Ministry of Science and Technology of Taiwan for financial support [grant number MOST 108-2112-M-110-003]. The scanning electron microscopy investigations were conducted in the SFU Joint Scientific Center supported by Ministry of Science and Higher

Education of the Russian Federation [state assignment number FSRZ-2020-0011]. X-ray diffraction data were obtained using analytical equipment of Krasnoyarsk Regional Center of Research Equipment of Federal Research Center “Krasnoyarsk Science Center SB RAS”.

Data availability statement

The processed data required to reproduce these findings cannot be shared at this time as the data also forms part of an ongoing study.

References

[1] H. Ohno, D. Chiba, F. Matsukura, T. Omiya, E. Abe, T. Dietl, Y. Ohno, K. Ohtani, Nature 408 (2000) 944–946, https://doi.org/10.1038/35050040.
[2] K. Sato, H. Katayama-Yoshida, Semicond. Sci. Technol. 17 (2002) 367–376, https://doi.org/10.1088/0268-1242/17/4/309.
[3] S.J. Pearton, W.H. Heo, M. Ivill, D.P. Norton, T. Steiner, Semicond. Sci. Technol. 19 (2004) R59–R74, https://doi.org/10.1088/0268-1242/19/10/R01.
[4] F. Pan, C. Song, X.J. Liu, Y.C. Yang, F. Zeng, Mater. Sci. Eng. R. 62 (2008) 1–35, https://doi.org/10.1016/j.mser.2008.04.002.
[5] X.H. Xu, H.J. Blythe, M. Ziese, A.J. Behan, J.R. Neal, A. Mokhtari, R.M. Ibrahim, A. M. Fox, G.A. Gehring, New J. Phys. 8 (2006) 135, https://doi.org/10.1088/1367-2630/8/8/135.
[6] H.-J. Lee, C.H. Park, S.-Y. Jeong, K.-J. Yee, C.R. Cho, M.-H. Jung, D.J. Chadi, Appl. Phys. Lett. 88 (2006), 062504, https://doi.org/10.1063/1.2171789.
[7] X.-C. Liu, E.-W. Shi, Z.-Z. Chen, H.-W. Zhang, B.-Y. Chen, L.-X. Song, S.-Q. Wei, B. He, Z. Xie, J. Crystal Growth 307 (2007) 14–18, https://doi.org/10.1016/j.jcrysgro.2007.05.050.
[8] C.-L. Tsai, Y.-J. Lin, C.-J. Liu, L. Horng, Y.-T. Shih, M.-S. Wang, C.-S. Huang, C.-S. Jhang, Y.-H. Chen, H.-C. Chang, Appl. Surf. Sci. 255 (2009) 8643–8647, https://doi.org/10.1016/j.apsusc.2009.06.040.
[9] Z.L. Lu, W. Miao, W.Q. Zou, M.X. Xu, F.M. Zhang, J. Alloys Compd. 494 (2010) 392–395, https://doi.org/10.1016/j.jallcom.2010.01.056.
[10] H. Sun, S.-C. Chen, C.-H. Wang, Y.-W. Lin, C.-K. Wen, T.-H. Chuang, X. Wang, S.-S. Lin, M.-J. Dai, Surf. Coat. Technol. 359 (2019) 390–395, https://doi.org/10.1016/j.surfcoat.2018.10.105.
[11] C.G. Van de Walle, Phys. Rev. Lett. 85 (2000) 1012–1015, https://doi.org/10.1103/PhysRevLett.85.1012.
[12] M.G. Wardle, J.P. Goss, P.R. Briddon, Phys. Rev. Lett. 96 (2006), 205504, https://doi.org/10.1103/PhysRevLett.96.205504.
[13] Y.C. Cho, S.-J. Kim, S. Lee, S.J. Kim, C.R. Cho, H.-H. Nahm, C.H. Park, I.K. Jeong, S. Park, T.E. Hong, S. Kuroda, S.-Y. Jeong, Appl. Phys. Lett. 95 (2009), 172514, https://doi.org/10.1063/1.3257733.
[14] C. Li, H. Liang, J. Zhao, Q. Fenga, J. Bian, Y. Liu, R. Shen, W. Li, G. Wu, G.T. Du, Appl. Surf. Sci. 256 (2010) 6770–6774, https://doi.org/10.1016/j.apsusc.2010.04.087.
[15] S. Lee, B.-S. Kim, S.-W. Seo, Y.C. Cho, S.K. Kim, J.P. Kim, I.I.-K. Jeong, C.R. Cho, C. U. Jung, H. Koinuma, S.-Y. Jeong, J. Appl. Phys. 111 (2012) 07C304, https://doi.org/10.1063/1.3671786.
[16] J.H. Park, S. Lee, B.-S. Kim, W.-K. Kim, Y.C. Cho, M.W. Oh, C.R. Cho, S.-Y. Jeong, Appl. Phys. Lett. 104 (2014), 052412, https://doi.org/10.1063/1.4864187.
[17] S.J. Kim, S.Y. Cha, J.Y. Kim, J.M. Shin, Y.C. Cho, S. Lee, W.-K. Kim, S.-Y. Jeong, Y. S. Yang, C.R. Cho, H.W. Choi, M.-H. Jung, B.-E. Jun, K.-Y. Kwon, Y. Kuroiwa, C. Moriyoshi, J. Phys. Chem. C 116 (2012) 2196–12202, https://doi.org/10.1021/jp300536w.
[18] S. Deka, P.A. Joy, Appl. Phys. Lett. 89 (2006), 032508, https://doi.org/10.1063/1.2227642.
[19] Y. Fukuma, F. Odawara, H. Asada, T. Koyanagi, Phys. Rev. B 78 (2008), 104417, https://doi.org/10.1103/PhysRevB.78.104417.
[20] H.S. Hsu, J.C.A. Huang, S.F. Chen, C.P. Liu, Appl. Phys. Lett. 90 (2007), 102506, https://doi.org/10.1063/1.2711763.
[21] A.D. Trolio, P. Alippi, E.M. Bauer, G. Ciatto, M.H. Chu, G. Varvaro, A. Polimeni, M. Capizzi, M. Valentini, F. Bobba, C.D. Giorgio, A.A. Bonapasta, ACS Appl. Mater. Interfaces 8 (2016) 12925–12931, https://doi.org/10.1021/acsami.6b04203.
[22] S. Yin, M.M. Shirolkar, J. Li, M. Li, X. Song, X. Dong, H. Wang, AIP Adv. 6 (2016), 065020, https://doi.org/10.1063/1.4954885.
[23] S.Y. Yang, B.Y. Mana, M. Liu, C.S. Chen, X.G. Gao, C.C. Wang, B. Hu, Appl. Surf. Sci. 257 (2011) 3856–3860, https://doi.org/10.1016/j.apsusc.2010.11.057.
[24] B.L. Zhu, J. Wang, S.J. Zhu, J. Wu, D.W. Zeng, C.S. Xie, J. Electro-chem Soc. 159 (2012) H536–H544, https://doi.org/10.1149/2.022206jes.
[25] I.S. Edelman, H. Chou, Yu.E. Samoshkina, D.A. Petrov, H.C. Lin, W.L. Chan, S.-J. Sun, S.M. Zharkov, G.V. Bondarenko, M.S. Platunov, A. Rogalev, J. Mag. Mag. Mater. 489 (2019), 165461, https://doi.org/10.1016/j.jmmm.2019.165461.
[26] B.P. Shantheyanda, K.B. Sundaram, N.S. Shiradkar, Mater. Sci. Eng. 177 (2012) 1777–1782, https://doi.org/10.1016/j.mseb.2012.08.026.
[27] Q. Huang, Y. Liu, S. Yang, Y. Zhao, X. Zhang, Sol. En. Mater. Sol. Cells 103 (2012) 134–139, https://doi.org/10.1016/j.solmat.2012.03.033.
[28] Y.R. Park, J. Kim, Y.S. Kim, Appl. Surf. Sci. 255 (2009) 9010–9014, https://doi.org/10.1016/j.apsusc.2009.06.083.
[29] S.C. Abrahams, J.L. Bernstein, Acta Cryst. B 25 (1969) 1233–1236, https://doi.org/10.1107/S0567740869003876.
[30] X.-L. Chen, J. Ming Liu, J. Ni, Y. Zhao, X. Dan Zhang, Appl. Surf. Sci. 328 (2015) 193–197, https://doi.org/10.1016/j.apsusc.2014.12.018.
[31] W.H. Breckenridge, J.-H. Wang, J. Chem. Phys. 87 (1987) 2630–2637, https://doi.org/10.1063/1.453101.
[32] K.Yu. Zhizhin, N.N. Mal’tseva, G.A. Buzanov, N.T. Kuznetsov, Russian J. Inorg. Chem. 59 (2014) 1665–1678, https://doi.org/10.1134/S003602361414006X.
[33] A. Shayesteh, D.R.T. Appadoo, I.E. Gordon, P.F. Bernath, J. Am. Chem. Soc. 126 (2004) 14356–14357, https://doi.org/10.1021/ja046050b.
[34] M. Kodu, T. Arroval, T. Avarmaf, R. Jaaniso, I. Kink, S. Leinberg, K. Savi, M. Timusk, Appl. Surf. Sci. 320 (2014) 756–763, https://doi.org/10.1016/j.apsusc.2014.08.138.
[35] O. Gürbüz, I. Kurt, S. Çalışkan, S. Güner, Appl. Surf. Sci. 349 (2015) 549–560, https://doi.org/10.1016/j.apsusc.2015.04.233.
[36] Marcel H.F. Sluiter, Y. Kawazoe, P. Sharma, A. Inoue, A.R. Raju, C. Rout, U. V. Waghmare, Phys. Rev. Lett. 94 (2005), 187204, https://doi.org/10.1103/PhysRevLett.94.187204.
[37] A. Janotti, C.G. Van de Walle, Nat. Mater. 6 (2007) 44–47, https://doi.org/10.1038/nmat1795.
[38] T. Ong, L. Xu, T.A. van der Laan, S. Xu, K. Ostrikov, Appl. Surf. Sci. 257 (2011) 9986–9990, https://doi.org/10.1016/j.apsusc.2011.06.121.
[39] S. Oktik, Prog. Cryst. Growth Charact. 17 (1988) 171–240, https://doi.org/10.1016/0146-3535(88)90006-8.
[40] M. Caglar, S. Ilican, Y. Caglar, F. Yakuphanoglu, Appl. Surf. Sci. 255 (2009) 4491–4496, https://doi.org/10.1016/j.apsusc.2008.11.055.
[41] R. Ghosh, D. Basak, S. Fujihara, J. Appl. Phys. 96 (2004) 2689–2692, https://doi.org/10.1063/1.1769598.
[42] L.-Y. Chen, W.-H. Chen, J.-J. Wang, F.C.-N. Hong, Y.-K. Su, Appl. Phys. Lett. 85 (2004) 5628–5630, https://doi.org/10.1063/1.1835991.
[43] J.C. Nie, J.Y. Yang, Y. Piao, H. Li, Y. Sun, Q.M. Xue, C.M. Xiong, R.F. Dou, Q.Y. Tu, Appl. Phys. Lett. 93 (2008), 173104, https://doi.org/10.1063/1.3010376.
[44] P.D.C. King, T.D. Veal, F. Fuchs, C.Y. Wang, D.J. Payne, A. Bourlange, H. Zhang, G. R. Bell, V. Cimalla, O. Ambacher, R.G. Egdell, F. Bechstedt, C.F. McConville, Phys. Rev. B 79 (2009), 205211, https://doi.org/10.1103/PhysRevB.79.205211.
[45] G. Shanmuganathan, I.B. Shameem Banu, Superlattices Microstruct. 75 (2014) 879–889, https://doi.org/10.1016/j.spmi.2014.08.024.
[46] J.M.D. Coey, J.T. Mlack, M. Venkatesan, P. Stamenov, IEEE Trans. Magn. 46 (2010) 2501–2503, https://doi.org/10.1109/TMAG.2010.2041910.
[47] J.M.D. Coey, M. Venkatesan, C.B. Fitzgerald, Nat. Mater. 4 (2005) 173–179, https://doi.org/10.1038/nmat1310.
[48] M. Ivill, S.J. Pearton, S. Rawal, L. Leu, P. Sadik, R. Das, A.F. Hebard, M. Chisholm, J.D. Budai, D.P. Norton, New J. Phys. 10 (2008), 065002, https://doi.org/10.1088/1367-2630/10/6/065002.
[49] F.-Y. Ran, M. Tanemura, Y. Hayashi, T. Hihara, J. Crystal Growth 311 (2009) 4270–4274, https://doi.org/10.1016/j.jcrysgro.2009.07.008.
[50] V.M. de Almeida, A. Mesquita, A.O. de Zevallos, N.C. Mamani, P.P. Neves, X. Gratens, V.A. Chitta, W.B. Ferraz, A.C. Doriguetto, A.C.S. Sabioni, H.B. de Carvalho, J. Alloys Compd. 655 (2016) 406–414, https://doi.org/10.1016/j.jallcom.2015.09.084.
[51] M.J. Calderon, S. Das Sarma, Ann. Phys. 322 (2007) 2618–2634, https://doi.org/10.1016/j.aop.2007.01.010.
[52] D. Mukherjee, T. Dhakal, H. Srikanth, P. Mukherjee, S. Witanachchi, Phys. Rev. B 81 (2010), 205202, https://doi.org/10.1103/PhysRevB.81.205202.